Journal of Rock Mechanics and Geotechnical Engineering 18 (2026) 3891–3903

Contents lists available at ScienceDirect

Journal of Rock Mechanics and Geotechnical Engineering

journal homepage: www.jrmge.cn

Full Length Article

Anti-seepage performance of polymer-enhanced three-layer cover system of landfill: Field monitoring and numerical modelling

Ming Min [a], Hefu Pu [a,*], Chao Zhou [b], Xiao He [c], Lusha Jiang [c], Shengyi Deng [c]

[a] State Key Laboratory of Intelligent Geotechnics and Tunnelling, College of Civil and Transportation Engineering, Shenzhen University, Shenzhen, 518060, China
[b] Department of Civil and Environmental Engineering, The Hong Kong Polytechnic University, 999077, Hong Kong, China
[c] School of Civil and Hydraulic Engineering, Huazhong University of Science and Technology, Wuhan, 430074, China

ARTICLE INFO

Article history:
Received 8 February 2025
Received in revised form
3 June 2025
Accepted 3 June 2025
Available online 4 September 2025

Keywords:
Landfill cover
Water percolation
Polymer-modified bentonite
Climatic conditions
Field monitoring

ABSTRACT

Landfill cover system plays a crucial role in reducing leachate generation by limiting rainwater infiltration. This paper evaluates the field performance of a polymer-enhanced three-layer cover system at a leather sludge dump site in Xinji city, China over a 1-year monitoring period. Waste soil (WS), sand-bentonite mixture (SB), and sand-polymer-bentonite mixture (SPB) were used as the low-permeability layer, respectively, in three test areas, above which the fine-grained cultivated soil and gravel were used in the top and middle layers to form a capillary barrier. During the 1-year monitoring period, the recorded cumulative rainfall was 452.1 mm, and the volumetric water content (VWC) at the top layer fluctuated significantly from 0.13 to 0.45 in response to rainfall and evaporation, but that of the low-permeability layer maintained stable for both cover SB and SPB. No water percolation was detected during the 1-year monitoring period. Furthermore, numerical simulations were carried out to assess the anti-seepage performance under more extreme climatic conditions (i.e., higher rainfall intensity and long-term deterioration of soil permeability). Numerical simulations corroborated the field observations that the SPB layer effectively minimized percolation even under extreme climatic conditions. For example, under the most unfavourable conditions, the computed annual percolation through the cover SPB was 4.7 mm, as low as 27.2% and 8.1% that through the cover SB (=17.3 mm) and WS (=57.9 mm). Overall, the results suggest that the polymer-enhanced three-layer soil cover is a promising alternative to traditional geomembrane-based covers and/or thick composite soil covers.

1. Introduction

The generation of industrial solid wastes, such as tailings, red mud, and phosphogypsum, presents significant environmental and geological challenges when improperly managed (Khan et al., 2022a; Wu et al., 2022; Guo et al., 2024a; Proia et al., 2024; Min et al., 2024). Landfilling remains the most practical, cost-effective, and widely adopted method for mitigating the environmental impacts of industrial solid wastes (Ng et al., 2015, 2019; Rowe et al., 2017; Zhan et al., 2020; Nanda and Berruti, 2021; Chen et al., 2022; Hersey and Power, 2023; Pu et al., 2024; Shi et al., 2024). In this context, landfill cover systems are crucial for reducing rainwater infiltration, minimizing leachate production, minimizing landfill gas emissions, and mitigating associated environmental risks (Feng et al., 2017; Xie et al., 2018; Zhan et al., 2020; Chetri et al., 2022; Li et al., 2022a; Wijekoon et al., 2022; Guo et al., 2024b; Qiu et al., 2024). Consequently, the design of an effective cover system with satisfactory anti-seepage performance is essential for advancing waste management practices.

So far, various cover systems have been developed, including monolithic soil covers (Bohnhoff et al., 2009; Pu et al., 2023; Min et al., 2023), capillary barrier covers (CBCs) (Harnas et al., 2014; Rahardjo et al., 2016; Zhan et al., 2020; Li et al., 2022b; Feng et al., 2025b), geomembrane-based covers (Divya et al., 2012; Cortellazzo et al., 2022; Fan et al., 2024), geosynthetic clay liner-based covers (Hosney and Rowe, 2013; Rowe, 2020; Khan et al., 2022b), and CBC-based multi-layered covers (Ng et al., 2015, 2024; Shaikh et al., 2019; Min et al., 2024). Among these, geomembrane-based covers, CBCs, and CBC-based multi-layered

* Corresponding author.
E-mail address: puhefu@szu.edu.cn (H. Pu).

Peer review under responsibility of Institute of Rock and Soil Mechanics, Chinese Academy of Sciences.

https://doi.org/10.1016/j.jrmge.2025.06.027

covers are widely adopted and extensively studied due to their good anti-seepage performance, making them the main choices for modern landfill covers (Ng et al., 2022; Liu et al., 2024). However, these three types of covers still have their drawbacks. For the geomembrane-based covers, although the geomembrane can provide excellent anti-seepage performance, it is susceptible to slope instability (i.e., slide), punctures, tears, and degradation in the long term (Fox et al., 2014; Ghazizadeh and Bareither, 2021). Furthermore, the extremely low water and gas permeability of geomembrane would completely isolate the ecological environment of landfill, presenting challenges to re-greening and reclamation. For the CBCs, although they have been demonstrated to be effective in reducing water percolation in arid and semi-arid climates, their performance in humid climates (with greater rainfall) is usually unsatisfactory (Khire et al., 2000; Albright et al., 2004; Ng et al., 2022; Min et al., 2024; Feng et al., 2025b). For the CBC-based multi-layered covers, such as three-layer inclined capillary barrier (Zhan et al., 2014) and three-layer soil cover (Ng et al., 2015, 2022), although they can mitigate some of the drawbacks associated with the geomembrane-based covers, they typically require a large soil thickness, i.e., generally in the range of 1–2 m, which may not be feasible in the areas with limited soil resources or on a relatively steep slope which is common in industrial waste dump site or landfill. Consequently, there is a critical need for a more reliable and efficient cover system.

Bentonite, a natural low-permeability clay, has been widely used for contaminants containment, particularly as the key material for anti-fouling barriers, such as geosynthetic clay liner and soil-bentonite mixture layer (Li et al., 2015; Feng et al., 2018, 2023a, 2025a; Rawat et al., 2019; Wang et al., 2022; He et al., 2022; Sun et al., 2022; Zhan et al., 2024; Shi et al., 2025). Although bentonite's permeability is very low (i.e., $<1 \times 10^{-10}$ m/s) and hence can reduce the thickness of the cover system, it is highly prone to cracking under freezing-thawing cycles and/or drying-wetting cycles, leading to substantial deterioration of the cover's servicing performance (Lin and Benson, 2000; Consoli et al., 2017; Rowe and Hamdan, 2022; Gahlot et al., 2022; Li et al., 2023; Chen et al., 2024). Furthermore, these deteriorations are further exacerbated in harsh landfill environments. For example, the leachates of industrial solid waste are typically characterized by extreme pH and/or high salt concentrations, thus significantly compromising the permeability of natural bentonite-based materials (Benson et al., 2018; Chen et al., 2018; Wang et al., 2022). Recently, studies on polymer-modified bentonite have presented performance superior to traditional, natural bentonite (Piqué et al., 2019; Wang et al., 2022; Cui and Chen, 2023; Fu et al., 2023; Jiang et al., 2025), including enhanced impermeability when encountering salt intrusion and/or drying-wetting cycles. In this study, a self-developed polymer-modified bentonite was mixed with sand and used as the low-permeability material for a polymer-enhanced three-layer cover system, thereby reducing the cover thickness while improving its resistance to cracking and salt intrusion, as well as improving its slope stability and sealing performance. However, previous studies have primarily focused on the anti-seepage performance of bentonite materials or were conducted under well-controlled laboratory conditions for short durations. The long-term durability and serviceability of the cover system constructed with these materials under natural climatic conditions remain unexplored, thus limiting their broader application.

The primary objective of this study is to investigate the effect of polymer inclusion on the long-term field performance of a three-layer cover system under natural climatic conditions. Field monitoring was conducted over one year, from 1 May 2023 to 1 May 2024, at a leather sludge dump site in Xinji, China. During this monitoring period, variations in volumetric water content, water percolation, and associated atmospheric parameters were continuously recorded. Additionally, numerical analyses were performed to evaluate the anti-seepage performance of the cover system, not only considering more extreme climatic conditions but also accounting for potential deterioration of the cover permeability caused by harsh environments.

2. Field monitoring program and instrumentation

2.1. Field description

The leather sludge dump site is located near Bailongqiu village, Xinji city, Hebei Province, China. Operations of sludge dumping started in December 2007, and the site was decommissioned in April 2008. The dumped sludge primarily originated from the leather wastewater treatment plant of Xinji city and was characterized by high salinity (maximum salt content of 63.5 g/kg), high organic matter (maximum 183 g/kg), and a bad smell. Tests revealed that total heavy metal concentrations, particularly chromium (i.e., concentration range 12800–24200 mg/kg) and zinc (i.e., concentration range 7200–14500 mg/kg), exceeded the relevant screening thresholds (i.e., 250 mg/kg for chromium and 300 mg/kg for zinc, according to the Chinese agricultural land pollution control standard "Soil environmental quality risk control standard for soil contamination of agricultural land", GB15618-2018). The site is situated in a semi-humid region, with rainfall occurring primarily between April and October. According to the local government's master plan, the site is designated for land reclamation after the sludge is solidified/stabilized in situ, and the site is contained by vertical cut-off walls and a cover barrier. To ensure the site can integrate with the surrounding farmland, the total thickness of the cover barrier is restricted to 0.7 m. Consequently, a three-layer soil cover was selected for the test area (Fig. 1), while other areas adopted geomembrane-based cover.

The layout of the test area is shown in Fig. 1. The field test area, measuring 72 m × 9 m, was divided into three test plots: WS, SB, and SPB. The primary difference among the three test plots is the composition of the low-permeability layer, i.e., the cover WS used fine-grained waste soil (i.e., excluding bentonite and polymer); the cover SB used the mixture of sand and bentonite; the cover SPB used the mixture of sand, bentonite, and a self-developed polymer (i.e., crosslinked polymer) as reported by Jiang et al. (2025). The cover system has an inclination angle of 3° to promote lateral diversion of rainwater. The cover system, with a total thickness of 0.7 m, consists of the following layers (from bottom to top, as shown in Fig. 1b): a 100-mm-thick low-permeability layer (comprised of WS, SB, or SPB), a 100-mm-thick gravel layer, and a 500-mm-thick fine-grained cultivated soil layer. Detailed properties of these materials will be introduced in the next section. To promote environmental sustainability, locally sourced waste soil was employed for the fine-grained soil layer in all test plots, and locally available gravel was used for the gravel layer. The soils were compacted layer by layer to achieve the desired degree of compaction (DOC) or relative density, viz., 85% DOC for cultivated soil, 93% DOC for low-permeability layer (i.e., waste soil, SB and SPB), and 95% relative density for gravel. Additionally, the mixed SB and SPB materials should be given 24 h to ensure complete hydration of the bentonite and polymer, before these mixtures are placed and compacted on site. To ensure good compaction for each soil layer, pre-compaction trial tests were conducted on site using different compactors and different compaction parameters (e.g., lift thickness, number of compactions each lift).

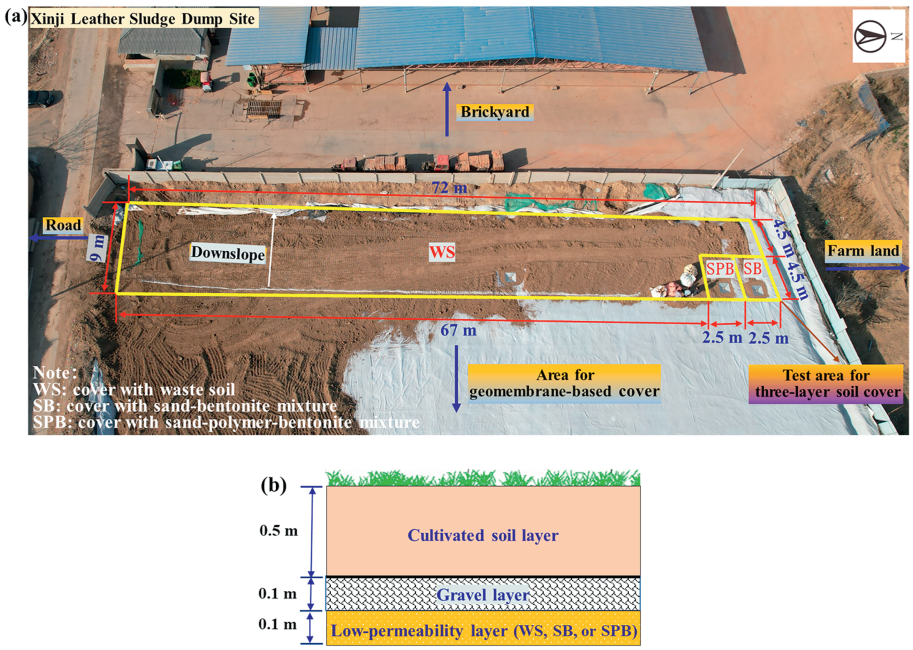

Fig. 1. The field test at the leather sludge dump site of Xinji city: (a) aerial view of the field test plot, and (b) configuration of the three-layer soil cover.

2.2. Material properties of the cover soils

Five types of cover materials were utilized in the field tests: cultivated soil, waste soil, gravel, sand-bentonite mixture, and sand-polymer-bentonite mixture. The waste soil was obtained from local engineering residues, while the gravel was locally purchased. The sand-bentonite mixture (SB) and sand-polymer-bentonite mixture (SPB) were developed independently (as seen in Fig. 2), in which the sand was well-graded and had the following particle size distribution: <0.075 mm (10%, identified as loess), 0.075–0.5 mm (35%), and 0.5–2 mm (55%). The SB mixture consisted of 85% well-graded sand (GS) and 15% bentonite, while the SPB mixture consisted of 85% GS, 14.5% bentonite, and 0.5% self-developed cross-linked polymer (following Jiang et al. 2022).

Fig. 2. (a) Preparation of the polymer powder (following Jiang et al., 2025), (b) mixing of the sand-polymer-bentonite (SPB) mixture on site and compaction, and (c) permeability coefficient test of the SPB samples after construction.

This polymer is primarily composed of monomers such as acrylic acid (AA), acrylamide (AM), and 2-acrylamido-2-methyl-1-propane sulfonic acid (AMPS). A crosslinker (i.e., N,N′-methylene bisacrylamide) and an initiator (i.e., potassium persulfate) are added to drive the cross-linking polymerization reaction, resulting in the formation of a cross-linked polymer network. This polymer has excellent swelling capacity even under a chemically aggressive environment, and thus can work together with the bentonite to effectively block the pores between the graded sand particles, giving the SPB material a low permeability. Furthermore, the vast majority (over 85%) of SPB well-graded sand, and its tight particle packing ensures the SPB's good bearing capacity (Proia et al., 2024). Also, note that the added polymer is in a small amount (0.5% only) and, more importantly, it does not have chemical reaction with (e.g., corrode or dissolve) the bentonite or sand particles and thus the SPB material will not collapse (Hosney and Rowe, 2017). The physical properties of these materials were determined according to the Soil Testing Methods standard (Ministry of Housing and Urban-Rural Development of the People's Republic of China, 2019) and summarized in Table 1.

The soil-water characteristic curve (SWCC), which illustrates the relationship between soil water content and matric suction (Dang et al., 2020), was obtained for the adopted soils using suction and moisture sensors combined with the filter paper method (ASTM D5298-16, 2016). The results are illustrated in Fig. 3a. The parameters that best fit the measured data were determined using the Van Genuchten (1980) model and expressed as Eq. (1), with the corresponding parameters listed in Table 2:

$$\frac{\theta_w - \theta_r}{\theta_s - \theta_r} = \left[\frac{1}{1 + (\alpha s)^n}\right]^m \tag{1}$$

where θ_w is the volumetric water content (VWC) of the tested soil, θ_s is the saturated VWC, θ_r is the residual VWC, s is the matric suction, and α, m, n are fitting parameters, where $m = 1–n^{-1}$.

The permeability coefficient (k_w) was predicted using the Van Genuchten (1980) equation, as shown in Fig. 3b. When the gravel is at a low degree of saturation (i.e., $s > 0.7$ kPa in Fig. 3b),

Table 1
Basic properties of the soils used in the present study.

Property	Soil type				
	Cultivated soil	Gravel	Low-permeability layer		
			Waste soil (WS)	Sand-bentonite mixture (SB)	Sand-polymer-bentonite mixture (SPB)
Specific gravity, G_s	2.66	2.45	2.67	2.7	2.7
Liquid limit, LL (%)	29.81		32.21		
Plastic limit, PL (%)	18.28		18.37		
Plasticity index, PI	11.53		13.73		
Maximum dry density, ρ_d (kg/m^3)	1758	1594	1765	1770	1720
Optimum moisture content (%)	15.5		16.2	17.8	17.8

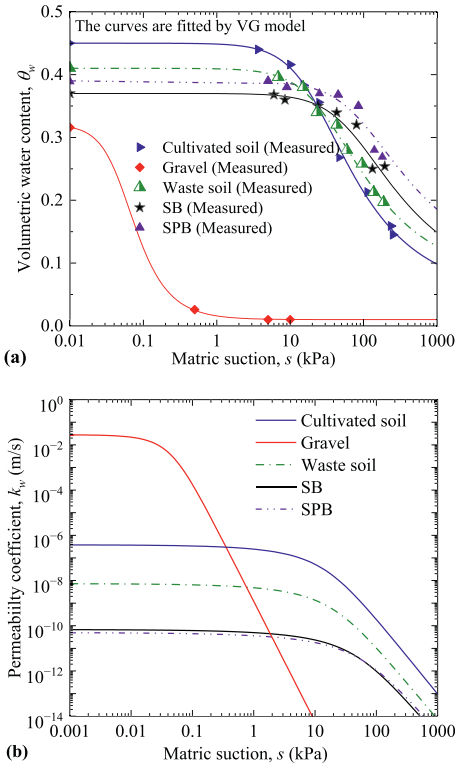

Fig. 3. Soil properties: (a) measured and fitted SWCC of various soils, and (b) predicted permeability coefficient functions of various soils using the Van Genuchten (1980) equation.

the permeability coefficient of gravel (i.e., drainage layer) was lower than that of cultivated soil (i.e., top layer), thereby forming a typical capillary barrier effect (Zhan et al., 2020; Guo et al., 2024b):

$$k_w = k_s \frac{\left[1 - \left(\alpha s^{(n-1)}\left(1 + (\alpha s)^{-m}\right)\right)\right]^2}{\left((1+\alpha s)^n\right)^{m/2}} \quad (2)$$

where k_w is the permeability coefficient of soil, and k_s is the saturated permeability coefficient of soil.

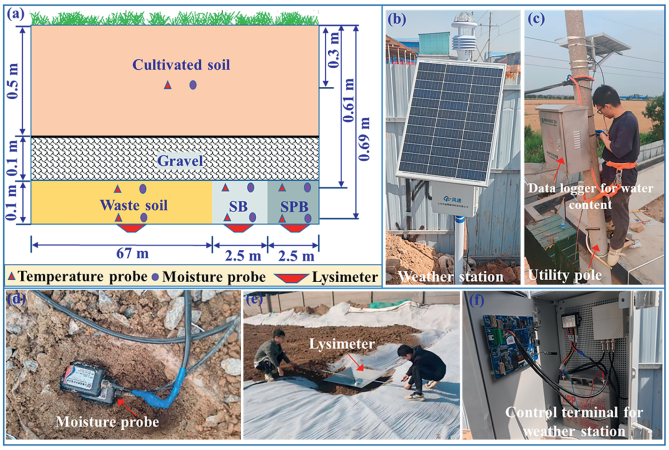

Fig. 4. Views of the layout of instrumentation and monitoring in the field.

2.3. Field instrumentation and monitoring

Once the in-situ solidification and stabilization of the leather sludge was completed, lysimeters were installed in three designated areas to monitor the amount of percolations, as shown in Fig. 4a and e. Each lysimeter, 1 m × 1 m in plan view, was connected to outlet pipes that directed water to a lower terrain outside the site, where water was collected in collection buckets. To facilitate long-term remote monitoring of percolation through the cover system, a submersible water level sensor (measuring accuracy = 1 mm, according to the manufacturer) was placed at the bottom of each collection bucket and connected to a data logger. To monitor the temporal and spatial variations of soil moisture and temperature within the cover, sensors (moisture probes and temperature probes, as shown in Fig. 4a) were embedded at different layers of the composite cover. Since future greening and farming activities can potentially damage the sensors in the shallow soil, only one sensor was installed in the cultivated soil layer (at a depth of 0.3 m), while two sensors were installed in the low-permeability layer (at depths of 0.61 m and 0.69 m). Prior to installation, all sensors were calibrated and connected to the

Table 2
Hydraulic properties of the materials used in this study.

Soil	Van Genuchten (1980) fitting parameters					Saturated permeability coefficient, k_s (m/s)
	θ_s	θ_r	α (kPa^{-1})	n	m	
Cultivated soil	0.45	0.05	0.05	1.54	0.35	3.8×10^{-7}
Gravel	0.32	0.01	19.6	2.33	0.57	2.8×10^{-2}
Waste soil	0.41	0.07	0.036	1.5	0.33	7.3×10^{-9}
SB mixture	0.37	0.06	0.015	1.46	0.32	6.8×10^{-11}
SPB mixture	0.39	0.08	0.012	1.43	0.3	4.98×10^{-11}

data logger. The data logger was housed in an electric box mounted on a utility pole at the perimeter of the leather sludge dump (as shown in Fig. 4c), capable of remotely recording water content data on an hourly basis. A weather station (Fig. 4b) was installed near the sludge dump site to measure the meteorological parameters, including rainfall, solar radiation, temperature, wind speed, and relative humidity. Data from the weather station were automatically logged in the control terminal (Fig. 4f), with real-time observation data downloadable from the cloud platform, which were then used for analysis and evaluation.

3. Field monitoring results

3.1. Seasonal variation of climate conditions

Fig. 5 shows the recorded atmospheric parameters during the one-year monitoring period from 1 May 2023 to 1 May 2024. As shown in Fig. 5a, the one-year cumulative rainfall was approximately 452.1 mm, consistent with the fact that the site is in a semi-humid climate region. The majority of the rainfall occurred between May and October, during which 373 mm of rainfall was recorded, accounting for ~82% of the annual rainfall. The highest daily rainfall (>55 mm) was recorded on 21 July 2023. Additionally, a long duration of drying (with daily rainfall <10 mm) was observed from November 2023 to May 2024.

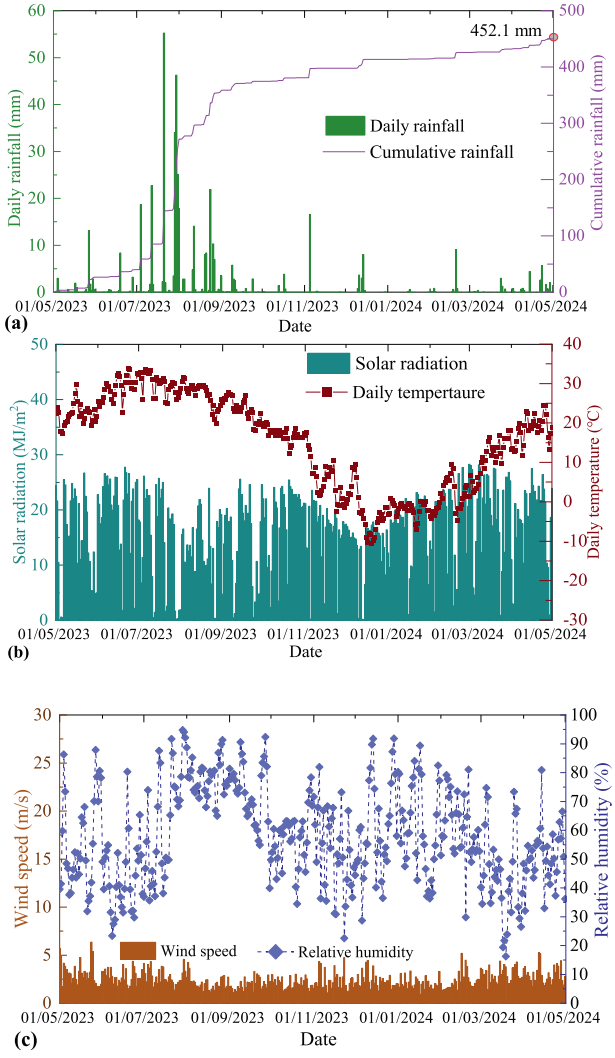

Fig. 5. Recorded atmospheric parameters during the one-year monitoring period: (a) daily rainfall and cumulative rainfall, (b) solar radiation and temperature, and (c) wind speed and relative humidity.

Fig. 5b shows that solar radiation at the dump site ranged from 5 MJ/m^2 to a maximum of 27 MJ/m^2. Atmospheric temperature measured by the weather station is presented in Fig. 5b. The average daily temperature in the area fluctuated between −9 °C and 33 °C, with lower temperatures observed during the dry winter season and higher temperatures during the wet summer season. Fig. 5c presents the recorded wind speed and relative humidity. Wind speeds near the soil cover varied from 2 m/s to 7 m/s, averaging 4 m/s. Generally, higher wind speed can enhance evaporation from the cover layer, reducing soil water content (Ng et al., 2022). Consequently, water infiltrated and stored in the cover system during wet seasons may be removed by the increased evaporation in dry periods, leading to reduced percolation. Throughout the monitoring period, relative humidity ranged from 20% to 95% without a consistent pattern. Generally, higher relative humidity can reduce evaporation and potentially increase percolation through the cover system.

3.2. Seasonal response of water content of the covers

During the monitoring period from 1 May 2023 to 1 May 2024, the volumetric water content (VWC) at various depths was measured for the three different covers (i.e., cover WS, cover SB, and cover SPB). Note that the moisture sensors in the cover WS were damaged by heavy machinery during the cover construction, and thus these data are not presented. As shown in Fig. 6, VWC near the cover surface (i.e., at 0.3 m depth) was primarily influenced by rainfall and evaporation. Initially, the VWC at a depth of 0.3 m = 0.22 for cover SB and = 0.23 for cover SPB; during the 1-year monitoring period, significant variations in VWC were observed at the 0.3 m depth, ranging from 0.13 to a saturation point of 0.45. Nonetheless, the changes in VWC at the low-permeability layer were relatively small (i.e., by less than 0.16 and 0.12 in SB and SPB, respectively), even under heavy rainfall and drought conditions. This small variation is consistent with the field results reported by Ng et al. (2022) and is attributed to the capillary barrier effect at the fine- and coarse-grained soils' interface (Feng et al., 2025b). During minor rainfall events (i.e., less than 10 mm), the capillary barrier effect prevented the VWC at depths of 0.61 and 0.69 m from varying significantly. However, during heavy rainfall (e.g., 21 July 2023), the capillary barrier effect only lasted a short period, and the cultivated soil layer quickly spiked to full saturation, after which the low-permeability SB and SPB layers effectively hindered further rainwater infiltration.

Fig. 6 also shows that, even during a long period of drought (e.g., ~ half a year from October 2023 to April 2024), the reduction of VWC in the SB/SPB layer was minimal (= less than 0.05). This is because the existence of upper CBC effectively retarded water loss in the bottom layer (Zhan et al., 2020; Chen et al., 2022; Guo et al., 2024b). Furthermore, drought conditions reduced VWC in the top soil layer (as seen in Fig. 6), which recovered the capillary barrier effect after the water breakthrough in the wet season (Zhan et al., 2020; Ng et al., 2023; Feng et al., 2025b). This result means that the three-layer cover system performed satisfactorily under complex and variable natural climate conditions, although it has a total thickness of only 0.7 m without geomembrane.

3.3. Response of water content to a one-day heavy rainfall

According to the China Meteorological Administration, the term "heavy rainfall" refers to a weather phenomenon

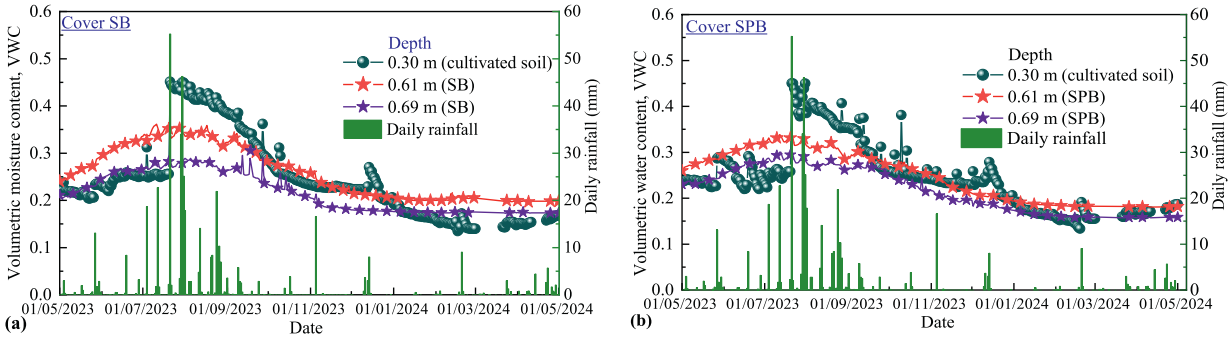

Fig. 6. Changes of VWC from 1 May 2023 to 1 May 2024 at different depths of: (a) cover SB, and (b) cover SPB.

characterized by substantial rainfall over a short duration (i.e., 24-h cumulative rainfall ≥50 mm). Based on this standard, only one heavy rainfall event was recorded during the 1-year monitoring period, with a total of 55.2 mm occurring on 21 July 2023. The temporal distribution of rainfall intensity during this event is shown in Fig. 7. This rainfall event exhibited significant temporal variability, with the majority of precipitation occurring in the middle portion of the day and the maximum hourly rainfall <11 mm/h.

Fig. 8 shows the changes in VWC of cover SB and cover SPB before and after this heavy rainfall event. As expected, the VWC in the shallow layer of the cover was significantly affected by the heavy rainfall. For example, at a depth of 0.3 m in the cultivated soil, the VWC of covers SB and SPB at 00:00 of 21 July 2023 were 0.258 and 0.255, respectively. At 24:00 of that day, both values increased to 0.45 for covers SB and SPB (increased by 74% and 76%, respectively). In the low-permeability layer, in contrast, the VWC changed minimally by the rainfall event. For example, at a depth of 0.61 m before the rainfall, the VWC of covers SB and SPB were 0.355 and 0.329, respectively, and increased only slightly to 0.359 and 0.33 after the rainfall (increased by 1.1% and 0.3%, respectively). These results suggest that the combined effects of the capillary break and the underlying low-permeability layer effectively reduced infiltration. Moreover, the SPB layer, which has even lower permeability than the SB layer (i.e., 4.98×10^{-11} m/s vs. 6.8×10^{-11} m/s), showed a negligible increase in VWC (by only 0.3%) under heavy rainfall.

3.4. Cumulative water percolation

Fig. 9 presents the cumulative water percolation through the covers WS, SB, and SPB during the one-year monitoring period. No

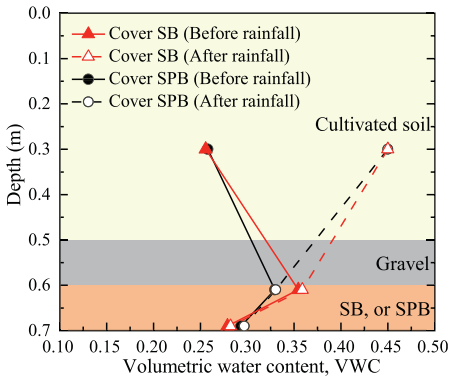

Fig. 8. Changes in VWC of cover SB and cover SPB before and after the heavy rainfall event on 21 July 2023.

percolation was detected during the one-year monitoring. As listed in Table 3, a comparison was made with the traditional CBCs and monolithic cover at five field sites in the USA and Germany (Warren et al., 1996; Melchior, 1997). Annual rainfall for CBCs and monolithic cover ranged from 539 mm to 911 mm, and the corresponding minimum and maximum annual percolations = 60 mm and 241 mm, respectively, substantially higher than the recommended value of 10 mm/year (Benson, 2002). It can be observed that the investigated three-layer cover has significantly smaller percolation than the traditional CBCs and monolithic cover in terms of either the total magnitude of percolation or its percentage of annual rainfall, although the three-layer cover has the smallest thickness. This comparison further demonstrates the effectiveness of the three-layer cover in preventing water percolation, although it does

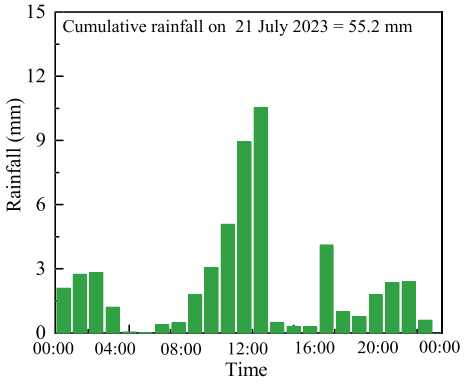

Fig. 7. Variation of rainfall with time on 21 July 2023.

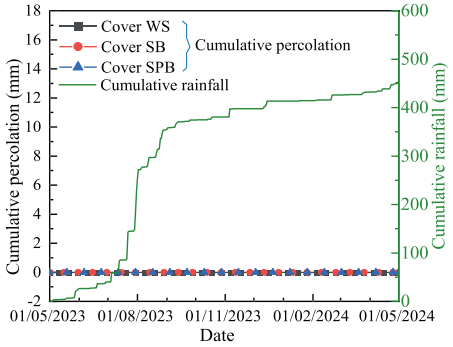

Fig. 9. Water percolation through covers WS, SB, and SPB from 1 May 2023 to 1 May 2024.

Table 3
Comparison of measured annual water percolation through the three-layer cover against the capillary barrier cover and the monolithic cover.

Reference	Location	Cover type	Cover thickness (m)	Annual rainfall (mm)	Percolation	
					Annual percolation (mm)	Percent of rainfall
This study	Xinji, China	Three-layer cover	0.7	452.1 882.3 (the wettest year in Xinji)	0 (Measured) 4.7 (Simulated for the wettest year)	0% 0.5%
Warren et al. (1996)	Utah, USA	Capillary barrier cover	1.8	539	80	15.4%
Benson et al. (2002)	Omaha, USA	Capillary barrier cover	1.36	617	60	9.8%
Melchior (1997)	Hamburg, Germany	Monolithic cover	1.8	865	65	7.5%
Barnswell and Dwyer (2012)	Georgia, USA	Monolithic cover	1.52	911	241	26.5%
Albright et al. (2004)	Iowa, USA	Monolithic cover	2.1	791	157	19.8%

not use a geomembrane and has a small total thickness.

4. Numerical study of the polymer-enhanced three-layer cover system under more extreme conditions

The field tests reported above have confirmed the excellent anti-seepage performance of the proposed cover system. However, since the climatic conditions during the one-year monitoring were not the most extreme in this region, and to address the limitation of insufficient on-site monitoring time (only one year), numerical simulations were conducted to further assess the cover system's anti-seepage performance. The simulations used the maximum rainfall condition in the city's history, and took into account the potential deterioration of the cover material. The numerical simulations were carried out in two stages. The first stage was to validate the numerical model against the field measurements. In the second stage, the validated numerical model was employed to investigate the effects of more extreme climatic conditions and permeability coefficient deterioration on the performance of the constructed three-layer cover.

4.1. Establishment of numerical model

In this study, Seep/W software (GeoStudio, Geo-Slope Int. Ltd.) was used to analyze the performance of the polymer-enhanced three-layer cover. Seep/W is a finite element software that accounts for variable climatic boundary conditions, surface ponding, and exchanges between the soil and atmosphere in both liquid and gaseous phases. Seep/W's feasibility and accuracy in simulating water flow in the vadose zone have been extensively validated (e.g., Razeghi et al., 2019; Wang et al., 2020; Rangarajan et al., 2024; Guo et al., 2024b).

Fig. 10 shows the model geometry and finite element mesh used in Seep/W. Previous studies have highlighted the critical role of mesh size in achieving convergence (Li et al., 2022c) and its impact on the accuracy of the transient seepage process in unsaturated soils (Vogel and Ippisch, 2008; Ng et al., 2023). In this present study, a balance between numerical accuracy and computational efficiency was achieved by setting the element discretization to 0.01 m and using a total of 14,000 rectangular elements. Fig. 10 shows the numerical model, which replicates the field test conditions (e.g., thickness = 0.7 m, slope angle = 3°, and consisting of three different soil layers: cultivated soil layer, gravel layer, and a bottom low-permeability layer).

The numerical modelling procedure in this study consisted of two stages: (i) initial steady-state seepage analysis and (ii) transient-state seepage analysis under natural climatic conditions. The steady-state seepage analysis was first conducted to determine the initial pore-water pressure distribution, which was subsequently used in the transient seepage analysis for both the validation and parametric studies. A minimal rainfall intensity of 0.001 mm/d was applied at the top boundary, as shown in Fig. 10, while the bottom boundary was defined as a constant water table (Ng et al., 2023). The right and left boundaries were both set as a no-flux boundary, except that the left boundary of the gravel layer was modelled as a free-drainage condition (Min et al., 2024).

After the steady-state seepage analysis, a transient-state seepage analysis was performed to simulate the water flow through the cover under natural climatic conditions. The specific boundary conditions for the transient analysis were as follows: the right and left boundaries remained the same as the steady-state analysis, the bottom boundary was changed to a potential seepage face, and the top boundary was modelled with land-climate interaction conditions. To compare with field test results, meteorological parameters monitored at the field site (shown in Fig. 4) were used. Additionally, meteorological data for the wettest year (i.e., 2021) of Xinji city's history, obtained from the local meteorological station, were applied for the parametric analyses. The cumulative rainfall for the wet year of 2021 amounted to 882.3 mm. The meteorological parameters are presented in Fig. 11, with data provided by the China Meteorological Data Service Center (https://data.cma.cn). It should be noted that, to assess the anti-seepage performance of the cover system under the most unfavourable conditions, numerical simulations deliberately excluded the evapotranspiration effect of vegetation. Additionally, the relevant vegetation parameters were not available on site, and thus the role of plant roots was not considered in this analysis.

In the parametric study, the transient seepage analysis was conducted by applying climate conditions immediately after the initial steady-state seepage analysis. The required input parameters, including the soil water characteristic curve (SWCC) and permeability coefficient (k_w), are detailed in Section 2.2, unless otherwise specified. The initial conditions for water transport in the Seep/W model are based on data recorded on 1 May 2023, after the completion of the field construction of the covers.

4.2. Verification of numerical model

Fig. 12a compares the simulated and measured VWCs before and after the heavy rainfall event on 21 July 2023. As shown, the simulated VWCs were slightly lower than the measured values, but overall a reasonably good agreement was obtained. At the end of the one-day rainfall, the VWC increased at all measured depths of the cover, and the simulated VWC near the surface of both cover SB

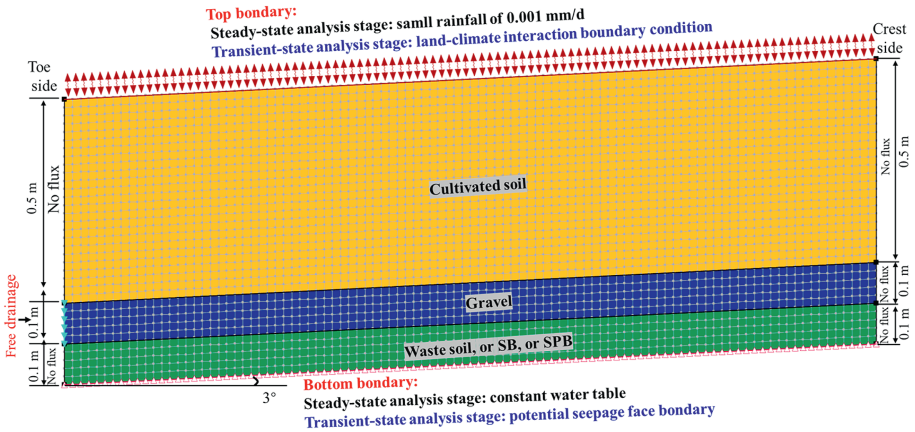

Fig. 10. Numerical model of the three-layer cover system.

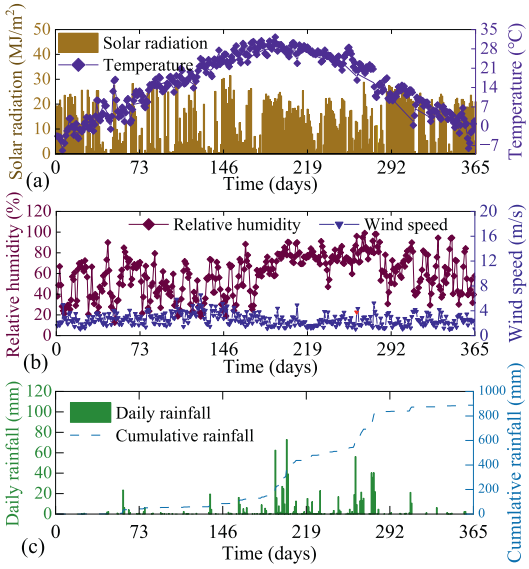

Fig. 11. Input climate data representing the local extreme climate condition for the numerical model: (a) solar radiation and temperature, (b) humidity and wind speed, and (c) rainfall.

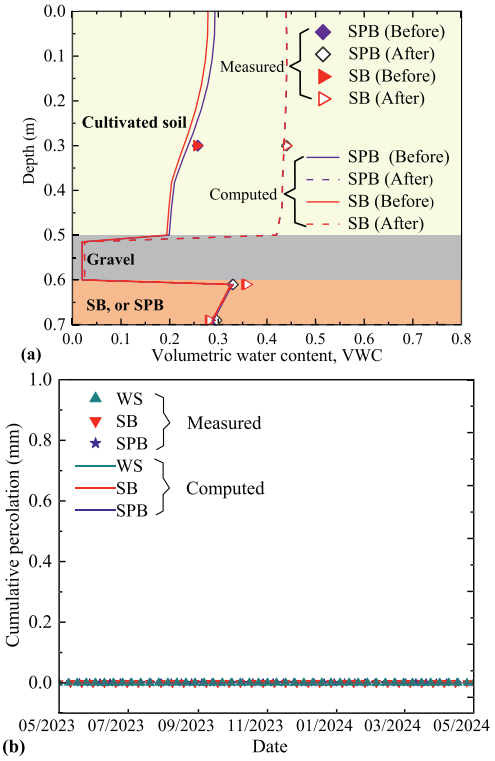

Fig. 12. Comparison of field measurements and numerical simulations: (a) VWC before and after the heavy rainfall on 21 July 2023, and (b) one-year cumulative water percolation through the covers.

and cover SPB approached saturation (saturation value = 0.45). The minor differences in the VWC of the low-permeability layers (SB vs. SPB) were observed, attributed to the difference in their saturated permeability coefficient. Fig. 12b presents the measured and simulated cumulative water percolation through covers WS, SB, and SPB from 1 May 2023 to 1 May 2024. The simulated cumulative percolation closely matched the field measurements (all were zero). The results in Fig. 12 confirm the validity of the established numerical model.

4.3. Simulation results of the constructed cover system during the wettest year of Xinji city's history

Climatic conditions can significantly affect the cover's anti-seepage performance. During the one-year field test, the Xinji leather sludge dump site did not encounter extreme rainfall conditions. To evaluate the cover's anti-seepage performance under extreme climate condition, seepage analysis was conducted in Seep/W by applying the climatic data of the wettest year (i.e., 2021) of Xinji city's history.

Fig. 13 presents the computed VWC and cumulative percolation of cover WS (Fig. 13a), cover SB (Fig. 13b), and cover SPB (Fig. 13c) under extreme climatic conditions (i.e., the wettest year of Xinji). As shown, the VWC in the shallow soil (e.g., depth of 0.05 m) fluctuated significantly in response to rainfall events and evaporation, varying between 0.05 and 0.45. In contrast, the VWC at greater depths (e.g., 0.4 m) showed relatively smaller and slower variations. Since July, frequent and intense rainfall resulted in a steady increase in VWC in the top layer, gradually reaching saturation and maintaining this saturated state for nearly 90 days. This condition was disrupted only in October due to reduced rainfall and ongoing evaporation. During the heavy rainfall events that occurred several times from 9 July 2021 to 15 October 2021, the

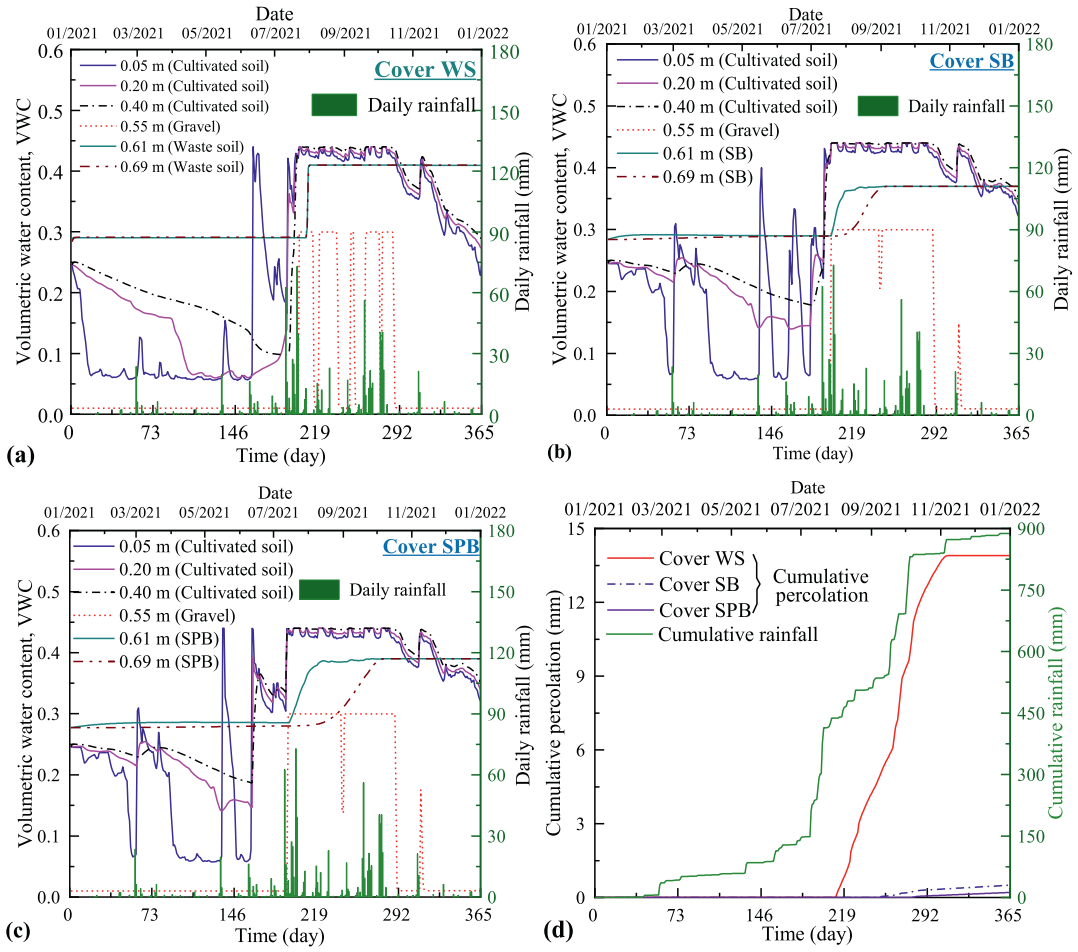

Fig. 13. Simulation results of the constructed cover system during the wettest year of Xinji city's history: (a) VWC of cover WS, (b) VWC of cover SB, (c) VWC of cover SPB, and (d) comparison of cumulative percolation.

VWC of the gravel layer increased quickly and significantly to full saturation, indicating that the capillary effect formed by the upper two layers was disrupted. Afterwards, further water infiltration was retarded by lateral diversion within the inclined gravel layer which is assisted by the blocking of the underlying low-permeability layer. The blocking/lateral diversion effects are closely related to the anti-seepage performance of the three-layer cover system, as shown by simulation results. For example, on 31 July 2021, the VWC of cover WS's low-permeability layer (i.e., waste soil) quickly reached saturation within only 1 day, indicating a limited blocking effect from waste soil. In contrast, cover SPB's low-permeability layer (i.e., sand-polymer-bentonite mixture) took as many as 60 days to reach saturation, indicating a strong blocking effect and thus gave the SPB cover an excellent anti-seepage performance.

Fig. 13d compares the annual cumulative water percolation through the three different cover systems. For covers SB and SPB, the cumulative percolations for the wettest year (i.e., annual rainfall = 882.3 mm) were as low as 0.2 mm and 0.5 mm, respectively, both significantly smaller than the recommended value of 10 mm/year by Benson et al. (2002). For cover WS, in contrast, the percolation began on day 211 and reached an annual cumulative value of 13.9 mm, approximately 66.2 times larger than that of cover SPB. Overall, Fig. 13 demonstrates that the proposed polymer-enhanced three-layer cover is highly effective in minimizing water percolation, although it has a small total thickness of only 0.7 m and does not use a geomembrane.

4.4. Simulation results of the constructed cover system considering the long-term deterioration of soil permeability

The numerical model used in this study assumed that soil permeability remained constant over time. However, existing studies in the literature have shown that factors such as wetting/drying cycles, freeze/thaw cycles, and/or microbial activities can significantly vary soil properties, especially the permeability coefficient k (Li et al., 2023; Zhang et al., 2024). To consider these variations, a detailed analysis was conducted considering the deterioration of soil k. After the leather sludge dump site is covered, the surface soil will typically require some loosening to support future reclamation and crop growth (Hamza and Anderson, 2005; Kuncoro et al., 2014; Feng et al., 2023b), causing the k of the surface soil to increase. For example, Kribaa et al. (2001) investigated the effects of various cultivation methods and climate conditions on the k of cultivated soil, finding that k ranged over two orders of magnitude from 7.12×10^{-7} m/s to 2.26×10^{-5} m/s. In the present study, the k of cultivated soil is 3.7×10^{-7} m/s measured upon on-site construction and is assumed to increase to 3.7×10^{-5} m/s to simulate the worst scenario. Additionally, for the low-permeability layer, its k may increase over time due to factors such as wetting/drying, freeze/thaw cycles, and salt intrusion. A wide range of k values have been reported in the literature for low-permeability soils. Table 4 summarises some existing studies in the literature on low-permeability soils. It is observed that, under the influence of

Table 4
Summary of the literature results on variations of permeability coefficient k caused by different factors.

Soil	Dry-wet cycles	Freeze-thaw cycles	Salt intrusion	References
cohesive soil	$8 \times 10^{-10} - 1.4 \times 10^{-7}$	$1 \times 10^{-8} - 5.5 \times 10^{-7}$	$5.4 \times 10^{-9} - 2.5 \times 10^{-7}$	Dalla Santa et al. (2020); He et al. (2015); Emmanuel and Anggraini (2020)
sand-bentonite mixture	$4.7 \times 10^{-11} - 6.9 \times 10^{-9}$	$4.7 \times 10^{-11} - 3.3 \times 10^{-9}$	$3.5 \times 10^{-11} - 8 \times 10^{-9}$	Yang et al. (2024); Namadi et al. (2023)
sand-modified bentonite mixture	$3.9 \times 10^{-11} - 2.1 \times 10^{-10}$	$3.9 \times 10^{-11} - 9.7 \times 10^{-11}$	$5 \times 10^{-11} - 2.2 \times 10^{-10}$	Yang et al. (2024); Hosney and Rowe (2017)

different factors, the k ranged from 8×10^{-10} m/s to 5.5×10^{-7} m/s for cohesive soil (>3 orders of magnitude), ranged from 3.5×10^{-11} m/s to 8×10^{-9} m/s for sand-bentonite mixture (>2 orders of magnitude), and ranged from 3.9×10^{-11} m/s to 2.2×10^{-10} m/s for sand-modified bentonite mixture (>1 order of magnitude). To consider the potential degradation, the k varied as follows in the present study: ranged from 7.3×10^{-9} m/s to 7.3×10^{-7} m/s for waste soil, ranged from 6.8×10^{-11} m/s to 6.8×10^{-9} m/s for SB, and ranged from 4.98×10^{-11} m/s to 4.98×10^{-10} m/s for SPB. As in section 4.3, extreme climate conditions were considered in this section by applying the climatic data from the wettest year of Xinji's history.

Fig. 14 presents the VWC and cumulative percolation at the cover bottom of covers WS, SB, and SPB during the wettest year of Xinji. For cover WS (Fig. 14a), the VWC at the cover bottom rapidly reached saturation due to frequent rainfalls and high k, leading to a significant increase in cumulative percolation. Specifically, when the k of waste soil deteriorated to 7.3×10^{-7} m/s, the cumulative percolation for cover WS exceeded 57.6 mm, failing to meet the recommended design value of 10 mm/year. This underscores that the traditional three-layer soil cover (without modified materials) needs adequate thickness to maintain good anti-seepage performance. For instance, Ng et al. (2022) proposed a three-layer cover system with a large total thickness of 1.8 m, and their system met the percolation requirement even in humid regions with a high annual rainfall of 2800 mm. However, this large thickness approach is not feasible for projects with strict thickness constraints (e.g., in the present study the total cover thickness is restricted to only 0.7 m to ensure that the covered site blends harmoniously with the surrounding farmland without sudden elevation change). In this case, the polymer-enhanced three-layer cover proposed in the present study provides an effective solution to this issue.

Furthermore, Fig. 14b and c presents the simulated results for

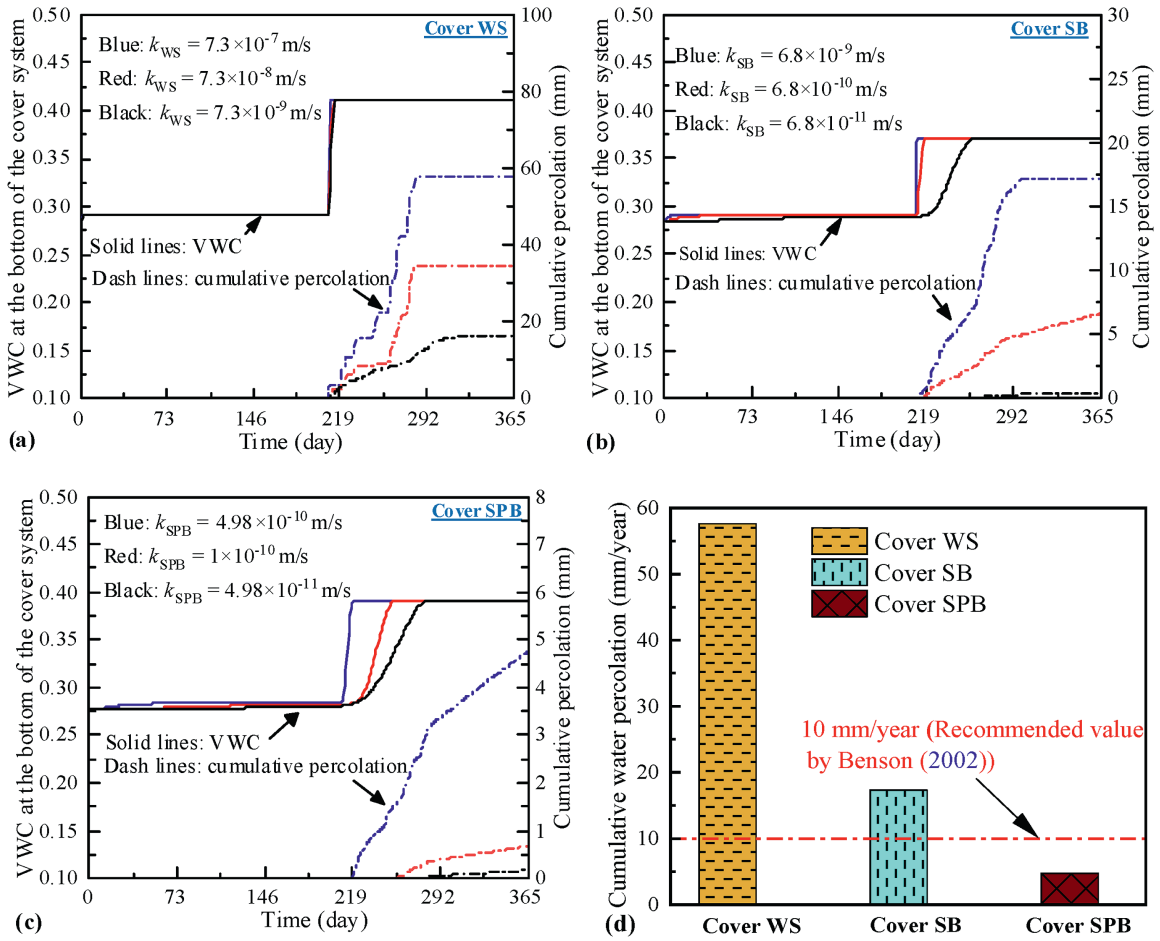

Fig. 14. Simulated cumulative percolation and VWC at the bottom of cover considering deterioration of soil permeability k during the wettest year in Xinji's history: (a) cover WS, (b) cover SB, (c) cover SPB, and (d) comparison of cumulative percolation of different covers.

covers SB and SPB, respectively. As the polymer addition helped the SPB layer maintain very low k_{SPB}, even under prolonged exposure to wet-dry cycles, freeze-thaw cycles and salt intrusion (Wang et al., 2022; Yang et al., 2024), a minimal water percolation through the cover was obtained. For instance, under adverse conditions (i.e., k_{SB} and k_{SPB} deteriorated to 6.8×10^{-9} m/s and 4.98×10^{-10} m/s, respectively), the simulated cumulative percolation was only 4.7 mm for cover SPB, representing a reduction of 72.8% and 91.8%, respectively, relative to 17.3 mm for cover SB and 57.6 mm for cover WS (Fig. 14d). Additionally, the simulated annual percolation for cover SPB is as small as less than 1% of the annual rainfall of 882.3 mm and is well below the 10 mm/year standard recommended by Benson et al. (2002). However, the annual percolation for cover SB no longer meets the recommended value. Even with a deteriorated (increased) k, cover SPB still exhibited the smallest percolation because its good resistance to wet-dry cycles, freeze-thaw cycles and salt intrusion led to the smallest increase in k. In sum, the proposed polymer-enhanced three-layer cover demonstrates significant potential for applications in humid regions with significant rainfall as well as in sites encountering high salinity and/or with strict cover thickness requirements.

5. Summary and conclusions

This study evaluated the anti-seepage performance of a polymer-enhanced three-layer soil cover at a leather sludge dump site in Xinji city, China. Field monitoring was conducted over one year, from 1 May 2023 to 1 May 2024, during which the VWC, temperature, and water percolation were recorded. Additionally, numerical simulations were performed to assess the performance of the three-layer cover under more extreme conditions (i.e., greater rainfall and long-term deterioration of soil permeability). The following conclusions can be drawn:

(1) Throughout the one-year monitoring period, no water percolation at the bottom of covers SB and SPB was detected, and the VWC of the cultivated soil layer fluctuated significantly due to rainfall and evaporation, ranging from 0.13 to 0.45. In contrast, the VWC of the low-permeability layer remained relatively stable, even under conditions of heavy rainfall or prolonged drought. Specifically, the maximum variation amplitude of the SB layer was 0.16, while that of the SPB layer was 0.12, reflecting a 33.3% decrease. The bottom low-permeability layer together with the capillary barrier effect formed by the upper cultivated soil layer and gravel layer significantly reduced water infiltration through the cover.

(2) Numerical simulations were conducted to consider the greatest rainfall intensity in Xinji's history as well as the significant increase/deterioration of soil permeability. The results further confirmed that the polymer-enhanced three-layer cover system was highly effective in reducing water percolation, even under the most unfavourable conditions. The simulated annual percolation of covers WS, SB, and SPB is 57.6 mm, 17.3 mm, and 4.7 mm, respectively. Only cover SPB met the recommended annual percolation criterion of 10 mm/year, with its simulated percolation <1% of the cumulative rainfall of 882.3 mm.

(3) Both field monitoring and numerical simulations demonstrated that the polymer-enhanced three-layer cover (with a total thickness of only 0.7 m) effectively reduced water percolation without using a geomembrane. These findings suggest that the polymer-enhanced three-layer cover offers a promising alternative to traditional thick soil or geomembrane-based covers.

CRediT authorship contribution statement

Ming Min: Investigation, Writing – review & editing, Writing – original draft, Data curation, Methodology, Resources. **Hefu Pu:** Funding acquisition, Writing – review & editing, Conceptualization, Supervision, Writing – original draft. **Chao Zhou:** Supervision, Writing – review & editing. **Xiao He:** Data curation, Investigation. **Lusha Jiang:** Investigation, Data curation. **Shengyi Deng:** Data curation, Investigation.

Data availability

Data will be made available on request.

Declaration of competing interest

The authors declare that they have no known competing financial interests or personal relationships that could have appeared to influence the work reported in this paper.

Acknowledgements

Financial support for this investigation was provided by the National Natural Science Foundation of China (Grant No. 52478351), Shenzhen Science and Technology Innovation Commission (Grant No. JCYJ20240813143306009), and GuangDong Basic and Applied Basic Research Foundation (Grant No. 2025A1515011843).

References

Albright, W.H., Benson, C.H., Gee, G.W., Roesler, A.C., Abichou, T., Apiwantragoon, P., Rock, S.A., 2004. Field water balance of landfill final covers. J. Environ. Qual. 33 (6), 2317–2332.

ASTM D5298-16, 2016. Standard Test Method for Measurement of Soil Potential (Suction) Using Filter Paper. ASTM, West Conshohocken, PA, USA.

Benson, C.H., Albright, W.H., Roesler, A.C., Abichou, T., 2002. Evaluation of final cover performance: field data from the alternative cover assessment program (ACAP). In: Proceedings Waste Management 02. Tucson, USA.

Benson, C.H., Chen, J.N., Edil, T.B., Likos, W.J., 2018. Hydraulic conductivity of compacted soil liners permeated with coal combustion product leachates. J. Geotech. Geoenviron. Eng. 144 (4), 04018011.

Bohnhoff, G.L., Ogorzalek, A.S., Benson, C.H., Shackelford, C.D., Apiwantragoon, P., 2009. Field data and water-balance predictions for a monolithic cover in a semiarid climate. J. Geotech. Geoenviron. Eng. 135 (3), 333–348.

Barnswell, K.D., Dwyer, D.F., 2012. Two-year performance by evapotranspiration covers for municipal solid waste landfills in northwest Ohio. Waste Manage 32 (12), 2336–2341.

Chen, C., Peng, W., Li, J., Luo, Q., Jiang, B., Yu, Y., Liu, E., 2024. Effects of freeze–thaw cycle on permeability and compression properties of aeolian soil–bentonite mixture. IJST-T. Civ. Eng. 48, 3621–3641.

Chen, J.N., Benson, C.H., Edil, T.B., 2018. Hydraulic conductivity of geosynthetic clay liners with sodium bentonite to coal combustion product leachates. J. Geotech. Geoenviron. Eng. 144 (3), 04018008.

Chen, R., Huang, J., Leung, A.K., Chen, Z., Chen, Z.K., 2022. Experimental investigation on water release and gas emission of evapotranspirative capillary barrier landfill covers. Soil Sci. Soc. Am. J. 86 (2), 311–323.

Chetri, J.K., Reddy, K.R., Grubb, D.G., 2022. Investigation of different biogeochemical cover configurations for mitigation of landfill gas emissions: laboratory column experiments. Acta Geotech 17 (12), 5481–5498.

Consoli, N.C., da Silva, K., Rivoire, A.B., 2017. Compacted clay-industrial wastes blends: long term performance under extreme freeze-thaw and wet-dry conditions. Appl. Clay Sci. 146, 404–410.

Cortellazzo, G., Russo, L.E., Busana, S., Carbone, L., Favaretti, M., Hangen, H., 2022. Field trial of a reinforced landfill cover system: performance and failure. Geotext. Geomembranes 50 (4), 655–667.

Cui, Q., Chen, B., 2023. Review of polymer-amended bentonite: categories, mechanism, modification processes and application in barriers for isolating contaminants. Appl. Clay Sci. 235, 106869.

Dang, M., Chai, J., Xu, Z., Qin, Y., Cao, J., Liu, F., 2020. Soil water characteristic curve

test and saturated-unsaturated seepage analysis in jiangcungou municipal solid waste landfill, China. Eng. Geol. 264, 105374.
Dalla Santa, G., Cola, S., Tateo, F., Galgaro, A., 2020. Hydraulic conductivity changes in compacted clayey barriers due to temperature variations in landfill top covers. Bull. Eng. Geol. Environ. 79, 2893–2905.
Divya, P.V., Viswanadham, B.V.S., Gourc, J.P., 2012. Influence of geomembrane on the deformation behaviour of clay-based landfill covers. Geotext. Geomembranes 34, 158–171.
Emmanuel, E., Anggraini, V., 2020. Effects of desiccation-induced cracking and leachate infiltration on the hydraulic conductivity of natural and olivine-treated marine clay. Int. J. Environ. Sci. Technol. 17, 2259–2278.
Fan, Y.H., Kerry Rowe, R., Brachman, R.W.I., Van Gulck, J., 2024. Impact of differential settlement on leakage through geomembranes in waste covers. Geosynth. Int. 32 (1), 82–93.
Feng, S.J., Chang, J.Y., Chen, H.X., 2018. Seismic analysis of landfill considering the effect of GM-GCL interface within liner. Soil Dyn. Earthquake Eng. 107, 152–163.
Feng, S.J., Ju, J.S., Zheng, Q.T., Zhang, X.L., Zhao, Y., 2025a. Modified approach for predicting seismic-induced deformation of landfills considering strength parameters of GMB-GCL interface within the liner system. Geotext. Geomembranes 53 (1), 247–259.
Feng, S., Huang, S.F., Jiang, J.L., Zhan, L.T., Li, G.Y., Guan, R.Q., Liu, H.W., 2023a. Effects of pore-size distribution on the gas diffusion coefficient and gas permeability of compacted manufactured sand tailing–bentonite mixtures. J. Geotech. Geoenviron. Eng. 149 (11), 04023101.
Feng, S., Huang, S.F., Ng, C.W.W., Chen, F.Q., Qian, X., Zhao, N.K., 2023b. Roots of Cynodon dactylon increase gas permeability and gas diffusion coefficient of highly compacted soils. Plant Soil 492 (1), 329–351.
Feng, S., Leung, A.K., Ng, C.W.W., Liu, H.W., 2017. Theoretical analysis of coupled effects of microbe and root architecture on methane oxidation in vegetated landfill covers. Sci. Total Environ. 599, 1954–1964.
Feng, S., Zheng, Y., Liu, H.W., Li, G.Y., Qian, X., 2025b. Numerical study of rainfall percolation through a novel capillary barrier cover with a zipper-shape interface between fine-and coarse-grained soils. Waste Manage 191, 220–229.
Fox, P.J., Thielmann, S.S., Stern, A.N., Athanassopoulos, C., 2014. Interface shear damage to a HDPE geomembrane. I: gravelly compacted clay liner. J. Geotech. Geoenviron. Eng. 140 (8), 04014039.
Fu, X.L., Zhuang, H., Reddy, K.R., Jiang, N.J., Du, Y.J., 2023. Novel composite polymer-amended bentonite for environmental containment: hydraulic conductivity, chemical compatibility, enhanced rheology and polymer stability. Constr. Build. Mater. 378, 131200.
Gahlot, R., Verma, A., Kumar, M., 2022. Geotechnical behavior of fly ash-coal ash and bentonite clay composite as a landfill barrier material with special emphasis on desiccation cracks. Environ. Res. 214, 113853.
Ghazizadeh, S., Bareither, C.A., 2021. Failure mechanisms of geosynthetic clay liner and textured geomembrane composite systems. Geotext Geomembr 49 (3), 789–803.
Guo, X., Zeng, M., Yu, H., Lin, F., Li, J., Wang, W., Chen, G., 2024a. Critical review for the potential analysis of material utilization from inorganic industrial solid waste. J. Clean. Prod. 459, 142457.
Guo, H.W., Ng, C.W.W., Zhang, Q., Qu, C., Hu, L., 2024b. Modelling the water diversion of a sustainable cover system under humid climates. J. Rock Mech. Geotech. Eng. 16 (7), 2429–2440.
Hamza, M.A., Anderson, W.K., 2005. Soil compaction in cropping systems: a review of the nature, causes and possible solutions. Soil Till. Res. 82 (2), 121–145.
Harnas, F.R., Rahardjo, H., Leong, E.C., Wang, J.Y., 2014. Experimental study on dual capillary barrier using recycled asphalt pavement materials. Can. Geotech. J. 51 (10), 1165–1177.
He, J., Wang, Y., Li, Y., Ruan, X.C., 2015. Effects of leachate infiltration and desiccation cracks on hydraulic conductivity of compacted clay. Water Sci. Eng. 8 (2), 151–157.
He, Y., Hu, G., Wu, D.Y., Zhu, K.F., Zhang, K.N., 2022. Contaminant migration and the retention behavior of a laterite–bentonite mixture engineered barrier in a landfill. J. Environ. Manag. 304, 114338.
Hersey, D., Power, C., 2023. Assessing water dynamics and net percolation rates within engineered cover systems for mine waste rock piles: a long-term field monitoring study. J. Hydrol. 627, 130471.
Hosney, M.S., Rowe, R.K., 2013. Changes in geosynthetic clay liner (GCL) properties after 2 years in a cover over arsenic-rich tailings. Can. Geotech. J. 50 (3), 326–342.
Hosney, M.S., Rowe, R.K., 2017. Performance of polymer-enhanced bentonite–sand mixture for covering arsenic-rich gold mine tailings for up to 4 years. Can. Geotech. J. 54 (4), 588–599.
Jiang, L.S., Wang, H., Miao, Y., Zhao, Q., Min, M., Qiu, J.W., Pu, H.F., 2025. Preparation and properties of crosslinked polymer/bentonite nanocomposite for containment of chemically aggressive liquids. J. Rock Mech. Geotech. Eng. https://doi.org/10.1016/j.jrmge.2025.04.008.
Khan, S., Anjum, R., Raza, S.T., Bazai, N.A., Ihtisham, M., 2022a. Technologies for municipal solid waste management: current status, challenges, and future perspectives. Chemosphere 288, 132403.
Khan, V., Roy, S., Rajesh, S., 2022b. Numerical investigation on hydraulic and gas flow response of MSW landfill cover system comprising a geosynthetic clay liner under arid climatic conditions. Geotext. Geomembranes 50 (6), 1159–1171.
Khire, M.V., Benson, C.H., Bosscher, P.J., 2000. Capillary barriers: design variables and water balance. J. Geotech. Geoenviron. Eng. 126 (8), 695–708.
Kuncoro, P.H., Koga, K., Satta, N., Muto, Y., 2014. A study on the effect of compaction on transport properties of soil gas and water I: relative gas diffusivity, air permeability, and saturated hydraulic conductivity. Soil Till. Res. 143, 172–179.
Kribaa, M., Hallaire, V., Curmi, P., Lahmar, R., 2001. Effect of various cultivation methods on the structure and hydraulic properties of a soil in a semi-arid climate. Soil Till. Res. 60 (1–2), 43–53.
Li, G.Y., Zhan, L.T., Zhang, S., Feng, S., Zhang, Z.H., 2022a. A dual-porosity model for coupled rainwater and landfill gas transport through capillary barrier covers. Comput. Geotech. 151, 104966.
Li, J., Chen, H., Gao, X., Ding, Q., Shan, W., Guo, H., Zhuo, J., 2023. Cracks evolution and micro mechanism of compacted clay under wet-dry cycles and wet-dry-freeze-thaw cycles. Cold Reg. Sci. Technol. 214, 103944.
Li, X.K., Li, X., Wang, F., Liu, Y., 2022b. The design criterion for capillary barrier cover in multi-climate regions. Waste Manage 149, 33–41.
Li, X., Li, X.K., Wu, Y.K., Wu, L.Z., Yue, Z.R., 2022c. Selection criteria of mesh size and time step in FEM analysis of highly nonlinear unsaturated seepage process. Comput. Geotech. 146, 104712.
Li, Y.C., Cleall, P.J., Wen, Y.D., Chen, Y.M., Pan, Q., 2015. Stresses in soil–bentonite slurry trench cut-off walls. Geotechnique 65 (10), 843–850.
Lin, L.C., Benson, C.H., 2000. Effect of wet-dry cycling on swelling and hydraulic conductivity of GCLs. J. Geotech. Geoenviron. Eng. 126 (1), 40–49.
Liu, H.W., Huang, Y., Feng, S., You, S.Q., Hong, Y., Shen, L.D., 2024. Experimental study of methane oxidation efficiency in three configurations of earthen landfill cover through soil column test. Waste Manage 190, 370–381.
Melchior, S., 1997. In-situ studies on the performance of landfill caps (compacted soil liners, geomembranes, geosynthetic clay liners, capillary barriers). Land Contam. Reclamat. 5 (3), 209–216.
Min, M., Pu, H.F., Feng, S., Qiu, J.W., Wen, X.J., 2023. Analytical solution for coupled water–gas transport in unsaturated landfill cover system with different root architectures. Comput. Geotech. 154, 105134.
Min, M., Pu, H.F., He, X., Deng, S.Y., 2024. Anti-seepage performance and oxygen barrier performance of the three-layered landfill cover system comprising neutralized slag under extreme climate conditions. Eng. Geol. 342, 107750.
Ministry of Housing and Urban-Rural Development of the People's Republic of China, 2019. Standard for Geotechnical Testing Method. China Jihua Press, Beijing (in Chinese).
Nanda, S., Berruti, F., 2021. Municipal solid waste management and landfilling technologies: a review. Environ. Chem. Lett. 19 (2), 1433–1456.
Namadi, A.H., Motlagh, A.H., Hassanlourad, M., Hosseinzadeh, M., 2023. Impact of heavy metal and carbonate on geotechnical properties of sand-bentonite mixtures. Indian Geotech. J. 53 (6), 1494–1504.
Ng, C.W.W., Chen, R., Coo, J.L., Liu, J., Ni, J.J., Chen, Y.M., Zhan, L.T., Guo, H.W., Lu, B.W., 2019. A novel vegetated three-layer landfill cover system using recycled construction wastes without geomembrane. Can. Geotech. J. 56 (12), 1863–1875.
Ng, C.W.W., Ng, C.L., Ni, J.J., Guo, H.W., Zhang, Q., Xue, Q., Chen, R., 2023. Analysis of a landfill cover without geomembrane using varied particle sizes of recycled concrete. J. Rock Mech. Geotech. Eng. 15 (5), 1263–1273.
Ng, C.W.W., Liu, J., Chen, R., Xu, J., 2015. Physical and numerical modeling of an inclined three-layer (silt/gravelly/sand/clay) capillary barrier cover system under extreme rainfall. Waste Manage 38, 210–221.
Ng, C.W.W., Guo, H.W., Ni, J.J., Chen, R., Xue, Q., Zhang, Y.M., Feng, Y., Chen, Z.K., 2022. Long-term field performance of non-vegetated and vegetated three-layer landfill cover systems using construction waste without geomembrane. Geotechnique 74 (2), 155–173.
Ng, C.W.W., Zhou, C., Ni, J.J., 2024. Advanced Unsaturated Soil Mechanics: Theory and Applications. CRC Press.
Piqué, T.M., Manzanal, D., Codevilla, M., Orlandi, S., 2019. Polymer-enhanced soil mixtures for potential use as covers or liners in landfill systems. Environ. Geotech. 8 (7), 467–479.
Proia, R., Salvatore, E., Croce, P., Modoni, G., 2024. Compacted sand–bentonite mixtures for the confinement of waste landfills. Acta Geotech 19, 8007–8022.
Pu, H.F., Min, M., Deng, S.Y., Wen, X.J., Xu, J., 2024. Transient analytical solution for coupled water–gas transport in unsaturated soil cover of landfill. J. Hydrol. 638, 131515.
Pu, H.F., Wen, X.J., Min, M., Chen, J.N., Qiu, J.W., 2023. Analytical solution for coupled water–gas transport in landfill cover. Acta Geotech 18, 4219–4231.
Qiu, P., Xu, Y., Yao, G., Liu, Y., Dong, L., Huang, Q., 2024. Deterioration modes, mechanisms, and effects of flexible landfill facilities disposing hazardous waste. J. Cleaner Prod. 451, 142030.
Rahardjo, H., Satyanaga, A., Harnas, F.R., Leong, E.C., 2016. Use of dual capillary barrier as cover system for a sanitary landfill in Singapore. Indian Geotech. J. 46, 228–238.
Rangarajan, S., Rahardjo, H., Satyanaga, A., Li, Y., 2024. Influence of 3D subsurface flow on slope stability for unsaturated soils. Eng. Geol. 339, 107665.
Rawat, A., Baille, W., Tripathy, S., 2019. Swelling behavior of compacted bentonite-sand mixture during water infiltration. Eng. Geol. 257, 105141.
Razeghi, H.R., Viswanadham, B.V.S., Mamaghanian, J., 2019. Centrifuge and numerical model studies on the behaviour of geogrid reinforced soil walls with marginal backfills with and without geocomposite layers. Geotext. Geomembranes 47 (5), 671–684.
Rowe, R.K., 2020. Geosynthetic clay liners: perceptions and misconceptions. Geotext. Geomembranes 48 (2), 137–156.
Rowe, R.K., Hamdan, S., 2022. Performance of GCLs after long-term wet–dry cycles under a defect in GMB in a landfill. Geosynth. Int. 30 (3), 225–246.

Rowe, R.K., Brachman, R.W., Hosney, M.S., Take, W.A., Arnepalli, D.N., 2017. Insight into hydraulic conductivity testing of geosynthetic clay liners (GCLs) exhumed after 5 and 7 years in a cover. Can. Geotech. J. 54 (8), 1118–1138.
Shaikh, J., Bordoloi, S., Yamsani, S.K., Sekharan, S., Rakesh, R.R., Sarmah, A.K., 2019. Long-term hydraulic performance of landfill cover system in extreme humid region: field monitoring and numerical approach. Sci. Total Environ. 688, 409–423.
Shi, Y., Xie, H.J., Wu, Y., Ci, M., Chen, X., 2024. Analytical study of water infiltration and contaminant transport in barrier systems. Water Res. 267, 122455.
Shi, Y.H., Xie, H.J., Ding, H., Wang, L., 2025. Contaminant transport through the heterogeneous GCL/SL composite liner: experimental and analytical studies. J. Hydrol. 651, 132607.
Sun, W., Liu, C., Yang, D., Sun, D., 2022. Evaluation of hydro-mechano-chemical behaviour of bentonite-sand mixtures. J. Rock Mech. Geotech. Eng. 14 (2), 637–652.
Van Genuchten, M.T., 1980. A closed-form equation for predicting the hydraulic conductivity of unsaturated soils. Soil Sci. Soc. Am. J. 44 (5), 892–898.
Vogel, H.J., Ippisch, O., 2008. Estimation of a critical spatial discretization limit for solving Richards' equation at large scales. Vadose Zone J. 7 (1), 112–114.
Wang, H., Jiang, L.S., Zhang, C., Wang, K., Li, Y.C., Pu, H.F., Zhao, Q., 2022. Ca-bentonite/polymer nanocomposite geosynthetic clay liners for effective containment of hazardous landfill leachate. Cleaner Prod 365, 132825.
Wang, L., Wu, C., Gu, X., Liu, H., Mei, G., Zhang, W., 2020. Probabilistic stability analysis of earth dam slope under transient seepage using multivariate adaptive regression splines. Bull. Eng. Geol. Environ. 79, 2763–2775.
Warren, R.W., Hakonson, T.E., Bostick, K.V., 1996. Choosing the most effective hazardous waste landfill cover. Remediat. J. 6 (2), 23–41.
Wijekoon, P., Koliyabandara, P.A., Cooray, A.T., Lam, S.S., Athapattu, B.C., Vithanage, M., 2022. Progress and prospects in mitigation of landfill leachate pollution: risk, pollution potential, treatment and challenges. J. Hazard. Mater. 421, 126627.
Wu, F., Ren, Y., Qu, G., Liu, S., Chen, B., Liu, X., Li, J., 2022. Utilization path of bulk industrial solid waste: a review on the multi-directional resource utilization path of phosphogypsum. J. Environ. Manag. 313, 114957.
Xie, H.J., Wang, Q., Bouazza, A., Feng, S.J., 2018. Analytical model for vapour-phase VOCs transport in four-layered landfill composite cover systems. Comput. Geotech. 101, 80–94.
Yang, W., Song, M.Y., Yuan, P., Liu, X.Y., Chen, W., Plé, O., 2024. Hydraulic conductivity of the polymer-modified bentonite-sand-phosphogypsum (PMB-S-PG) mixture under drying-wetting and freezing-thawing cycles. J. Mater. Cycles Waste Manage. 26, 1012–1026.
Zhan, L.T., Feng, T., Ni, J.Q., Feng, S., 2024. Hydrological response and crack resistance of polypropylene-fiber reinforced compacted steel slag-bentonite mixtures under wetting–drying cycles. Waste Manage 187, 252–261.
Zhan, L.T., Li, G.Y., Jiao, W.G., Lan, J.W., Chen, Y.M., Shi, W., 2020. Performance of a compacted loess/gravel cover as a capillary barrier and landfill gas emissions controller in Northwest China. Sci. Total Environ. 718, 137195.
Zhan, T.L., Li, H., Jia, G.W., Chen, Y.M., Fredlund, D.G., 2014. Physical and numerical study of lateral diversion by three-layer inclined capillary barrier covers under humid climatic conditions. Can. Geotech. J. 51 (12), 1438–1448.
Zhang, Z., Bao, W., Tian, L., Huang, Z., Chen, R., 2024. Study on the effect of pore structure changes induced by freeze-thaw-wetting-drying cycles on water retention characteristics of compacted loess. Constr. Build. Mater. 455, 139213.

Hefu Pu is a professor at Shenzhen University. His main research fields include containment and remediation of contaminated sites, disposal and beneficial reuse of waste materials, improvement of soft soil (mud), and energy geotechnics. He has served as Principal Investigator (PI) for many research funds, including National Key R&D Program of China, general grants of National Natural Science Foundation of China, and others. He has published more than 70 peer-reviewed academic papers, including many top journal papers. His research outcome has been applied in various engineering projects and received multiple research awards, including First Prize of Science and Technology Progress Award of Shanxi Province of China, First Prize of Science and Technology Progress Award of Hubei Province of China, and Excellent Paper Award by International Association for Computer Methods and Advances in Geomechanics.